Journal of Sound and Vibration (1997) **207**(4), 453–464

PREDICTION OF ROTOR HIGH-SPEED IMPULSIVE NOISE WITH A COMBINED CFD–KIRCHHOFF METHOD

S. Lee and J. Kim

Department of Aerospace Engineering, Seoul National University, Seoul, Korea

AND

Y. H. Yu and M. P. Isom

NASA Ames Research Center, Moffett Field, Ca, U.S.A.

(*Received* 12 *June* 1996, *and in final form* 14 *March* 1997)

A combined Computational Fluid Dynamics(CFD)–Kirchhoff method is presented for predicting high-speed impulsive noise generated by a rotor in hover. Two types of Kirchhoff integral formulas are used: one of them is a classical linear Kirchhoff formulation and the other a non-linear Kirchhoff formulation. An Euler finite-difference solver is executed first, from which a flow field is obtained to be used as an input to the Kirchhoff formulation to predict the acoustic far-field. The calculations are performed at Mach numbers of 0·90 and 0·95 to investigate the effectiveness of the linear and non-linear Kirchhoff formulas for delocalized flow. During these calculations, the retarded time equation is also carefully examined, in particular, for the cases where a control surface is located outside the sonic cylinder, for which multiple roots are obtained. Predicted results of acoustic far-field with the linear Kirchhoff formulation agree well with the experimental data when the control surface is at a particular location ($R_{cs}/R = 1{\cdot}46$), but the correlation weakens as it moves away from this specific location of the control surface due to the delocalized non-linear aerodynamic flow field. Calculations based on the non-linear Kirchhoff equation using the sonic cylinders as the control surfaces show reasonable agreements with the experimental data in the negative amplitudes for both tip Mach numbers of 0·90 and 0·95, except for some computational integration problems over a shock. It can be concluded that a non-linear formulation is necessary if the control surface is close to the blade and the flow is delocalized.

© 1997 Academic Press Limited

1. INTRODUCTION

High-speed impulsive rotor noise has been identified as one of the major noise sources generated by a rotor in high forward speed. The main mechanism has been attributed to transonic flow field around a blade tip in the advancing side. The prediction capability for this high-speed impulsive noise has been developed with varying degrees of success by many researchers. These prediction analyses have been mostly based on the acoustic analogy, called the Ffowcs Williams and Hawkings(FW–H) formulation [1], in which monopoles and dipoles are used for various applications with different rotor systems and speed ranges.

For a blade tip Mach number below the critical Mach number, the monopole and dipole representation provides fairly good results compared with the experimental data. In the high tip Mach number range, the monopole and dipole representation underpredicts the measured acoustic amplitude and does not predict the proper acoustic waveforms,

0022–460X/97/440453 + 12 $25.00/0/sv971069 © 1997 Academic Press Limited

particularly when a strong shock wave is present. Past the delocalization Mach number, the non-linear quadrupole term has been used to represent the non-linear flow field [2–5]. However, since this quadrupole term has a volume integral, the proper analytical modelling for this term turns out to be extremely difficult. Even though currently available acoustic representations of this quadrupole term may not be quite accurate physically and mathematically, this quadrupole representation has substantially improved the acoustic prediction capability in recent years. That is, the acoustic waveform and its amplitude seem to be better predicted when the quadrupole term is included. However, this acoustic quadrupole modelling is not quite mature for the high transonic speed range, and many questions remain to be resolved such as non-linear acoustic wave propagation [6, 7].

Another way to predict the sound field is by using a CFD method. Without using the acoustic analogy, a CFD solver has extended its computational domain to the acoustic far-field, in addition to solving the aerodynamic near-field. An Euler solver has been used to solve two dimensional blade-vortex interaction noise [8] and recently to predict the noise field generated by a non-lifting rotor at high hover Mach numbers [9]. This CFD method provides a rich numerical database, from which acoustic wave formation and propagation through the non-linear flow field can be examined in detail. Even though CFD solvers have been used extensively to predict the blade surface pressure distribution, these solvers are not suitable for predicting the acoustic radiation over regions far from the blade tip. The grid densities are insufficient to resolve the details of the acoustic far-field and numerical viscosity will generate computational instability problems. However, a potential advantage of CFD applications to helicopter acoustics is that acoustic pressure waves propagate to the far field along characteristic lines, and grid densities can be massed accordingly [9, 10].

An alternative way to take advantage of the near field CFD capability and far field acoustic analogy formulation is a combined CFD and Kirchhoff formulation [10, 11]. That is, a CFD solver is used to calculate the flow field near the blade and then this flow field information is used in a Kirchhoff formulation as an input. This combined CFD–Kirchhoff method is the main theme of this investigation. In this paper, a three-dimensional unsteady compressible Euler solver is used to calculate the flow field near the blade. Then, this flow field is used first in the classical linear Kirchhoff formulation to predict the acoustic far field. This linear formulation has two basic assumptions. First, the control surface should be large enough to contain all the non-linear aerodynamic flow field, which may be extended to the far field for delocalized flow. And secondly the sound propagation speed is assumed constant, and so the effect of the non-linear flow field on sound propagation is neglected.

In order to resolve these problems for the linear Kirchhoff formulation, a non-linear Kirchhoff formulation has been developed by Isom [12]. This non-linear formulation is an integral representation of the pressure and velocity on the control surface located at the linear sonic cylinder and the representation contains all the non-linear effects inside the control surface by converting the non-linear volume integral to the surface integral. One of the big advantages of this nonlinear formulation is the close proximity of the sonic surface to the rotor tip, so a CFD code is needed to resolve only the near-field region.

This paper compares the results of the linear formulation over several control surface locations (inside and outside of the sonic cylinder) and non-linear Kirchhoff formulas. The retarded time equation of these formulas is carefully examined due to the supersonic nature of the problem for control surfaces located beyond the sonic cylinder. The predicted acoustic results will be compared with available hover test data at Mach numbers of 0·90 and 0·95. The observer location is fixed with a distance of 3·09 times the rotor radius from the hub and the azimuth angle on the stationary Kirchhoff surface is defined as shown in Figure 1.

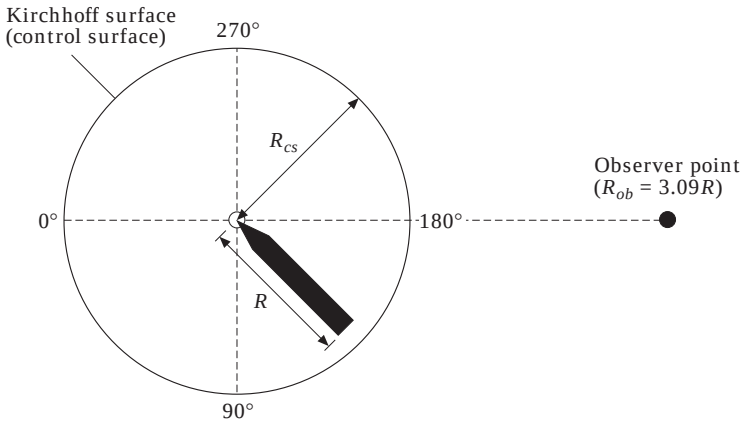

Figure 1. Schema of high-speed impulsive noise measurement set-up.

2. LINEAR KIRCHHOFF FORMULATION

Kirchhoff integral formula for a stationary control surface is the analytical expression of Huygens' principle [13]. The Kirchhoff equation is

$$p(\check{\mathbf{x}}, t) = \frac{1}{4\pi} \int\int_S \left[\frac{\cos\theta}{r^2} p - \frac{1}{r} \frac{\partial p}{\partial n} + \frac{\cos\theta}{a_\infty r} \frac{\partial p}{\partial \tau} \right] \mathrm{d}S(\check{\mathbf{y}}, \tau), \tag{1}$$

where p is the perturbed pressure; $(\check{\mathbf{x}}, t)$ are the observer's location and time: $(\check{\mathbf{y}}, \tau)$ are the source location and retarded time variables; θ is the angle between the normal vector $(\check{\mathbf{n}})$ on the surface and the radiation vector $(\check{\mathbf{r}})$; r is the distance between a source at the retarded time and an observer; a_∞ is the speed of sound. Note that pressure and its derivatives are evaluated at the retarded time. This formulation has been extended to moving surfaces [14] and used for aeroacoustic calculations such as transonic blade-vortex interaction noise [15–16]. A list of nomenclature is provided in the index.

The advantages of this formulation are; (1) it is expressed in terms of a surface integral, (2) all terms are linear, and (3) sound propagation speed is constant. One disadvantage is that the control surface should be large enough to contain the entire non-linear aerodynamic flow field. This requirement may generate a problem for the cases where the non-linear flow field is extended to the far field such as delocalized flow. Another disadvantage is that the effect of the non-linear flow field beyond the control surface on sound propagation is not included in this formulation.

3. RETARDED TIME SOLUTION FOR SUPERSONIC RANGE

The retarded time equation, even though it appears simple and benign, plays a very important role in calculating equation (1) and extreme care should be taken in obtaining its roots, particularly for the case of a control surface located outside of the sonic cylinder, where multiple roots exist [17]. The multiple roots of the retarded time equation seem to be an inevitable consequence of placing the control surface outside the sonic cylinder.

The multiple roots of the retarded time equation can be explained in the following manner. The relationship of the retarded time with the observer time is as follows

$$\tau = t - R/a_\infty, \tag{2}$$

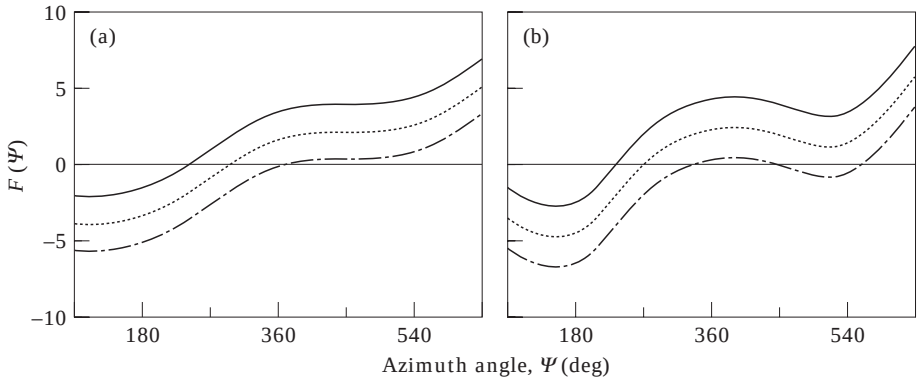

Figure 2. Retarded time solutions of sources for subsonic and supersonic control surface locations at $M_{tip} = 0{\cdot}90$ for R_{cs}/R ratios. (a) 1·05, (b) 2·41. Key for Ψ_1 values: ——, 240; · · · ·, 300; –·–·–, 360.

where R is the distance between a source position at the sound generation time and an observer at the sound receiving time. In order for sound waves generated from any two separate sources on the control surface to reach the observer simultaneously, the following equation should be satisfied.

$$R_1(\tau_1)/a_\infty + \Psi_1(\tau_1)/\Omega = R_2(\tau_2)/a_\infty + \Psi_2(\tau_2)/\Omega = t, \tag{3}$$

where R_1, R_2 are distances from the sources to the observer, Ψ_1, Ψ_2 are the respective azimuth angles of the source positions at the sound generation time, and Ω is an angular speed of the blade. For a given angle Ψ_1, the position of the second source Ψ_2 can be found by

$$F(\Psi) = -(\Omega/a_\infty)(R_1 - R_2) + \Psi_2 - \Psi_1 = 0. \tag{4}$$

The behavior of the function $F(\Psi)$ of equation (4) is illustrated in Figure 2, where two distinctive features of equation (4) in the subsonic and supersonic ranges are shown. That is, the solution of equation (4) for a subsonic range has only one root all the time (Figure 2(a)), while it has multiple roots for a supersonic range (Figure 2(b)).

4. NON-LINEAR KIRCHHOFF FORMULATION

The non-linear Kirchhoff formulation for acoustic pressure is given as [12],

$$\begin{aligned} p(\beta, t) = &-\frac{6^{1/3}\rho_0 a_\infty^2 M_{tip}^2 \varepsilon}{18\pi\beta} \iint_S \frac{V_r(T, Z_0) - V_r(\lambda, Z_0)}{T - \lambda} \frac{\mathrm{d}\lambda\, \mathrm{d}Z_0}{|T - \lambda|^{2/3}} \\ &+ \frac{6^{2/3}\rho_0 a_\infty^2 M_{tip}^2 \varepsilon}{36\pi\beta} \iint_S \frac{P(T, Z_0) - P(\lambda, Z_0)}{T - \lambda} \frac{\mathrm{sgn}\,(T - \lambda)}{|T - \lambda|^{1/3}} \mathrm{d}\lambda\, \mathrm{d}Z_0 \\ &- \frac{6^{1/3}\rho_0 a_\infty^2 (\gamma + 1) M_{tip} \varepsilon}{36\pi\beta\dot{g}} \iint_S \frac{p^2(T, Z_0) - P^2(\lambda, Z_0)}{T - \lambda} \frac{\mathrm{d}\lambda\, \mathrm{d}Z_0}{|T - \lambda|^{2/3}}, \end{aligned} \tag{5}$$

where pressure $p(\beta, t)$ is non-dimensional and transonically scaled by $\rho_0 a_\infty^2 \varepsilon^{2/3}$; V_r is the radial velocity scaled by $\Omega R\varepsilon$; ρ_0 and a_∞ are density and speed of sound in undisturbed air; γ is the ratio of specific heat; M_{tip} is blade tip Mach number; ε is the inverse of the

aspect ratio; β is the distance to an observer along a line tangent to the sonic cylinder and is defined as $\beta = [(\Omega R_{ob}/a_0)^2 - 1]^{1/2}$; Ω is the angular speed; R_{ob} is the distance from the hub to the observer; Z_0 is the vertical distance scaled by $\varepsilon^{2/3} a_\infty/\Omega$; T is a phase variable defined as $T = (1/\varepsilon)(\theta + \beta - \tan^{-1}\beta)$; θ is the cylindrical polar angle in a blade-fixed co-ordinate in radians; λ is the integration variable defined as the negative of x/c, where x is the blade co-ordinate; $\dot{g} = \tan\theta_s/M_{tip}$, where θ_s is the angle between the vector normal to the sonic circle and a shock.

The surface integrals in equation (5) are taken over the entire sonic plane, which is normal to the blade span-axis and tangent to the linear sonic cylinder. Equation (5) is the result of transforming the second order non-linear small disturbance potential equation to an integral equation. The conversion is accomplished by an elementary use of generalized functions and proceeds very much as in the derivation of the more general FW–H equation. There are three surface integrals, denoted as the V_r, P, P^2 terms. They are analogues, respectively, of the monopole, dipole, and quadrupole integrals that appear in various FW–H type equations. The novel feature of this equation is the appearance of the quadrupole term, which is originally a volume integral, as a surface integral. The reduction of volume integration to surface integration is based on several assumptions. The first (and main) assumption is that the derivative of disturbance pressure normal to the sonic plane is much smaller than its derivative tangent to the sonic plane. The tangential derivative is essentially a time derivative through the rapidly varying pressure waveform. The second assumption is that the curvature of the shock or characteristic surface in the direction normal to the plane of rotation is small off the blade tip and near the sonic plane. This assumption is based on the fact that a shock off the blade tip (in delocalized flow) is transonic: the Mach number of the flow relative to the shock is only slightly greater than one, and so the shock is nearly plane.

Equation (5) has several remarkable properties. In the case of delocalized flow, with a shock extending from the blade tip into the far field, each of the three integrals is singular as the phase variable T approaches the shock from either side. This means that when any one of the surface integrals is numerically evaluated in isolation from the other two, it will fail as T approaches the shock. The same singular behavior results when any two of the integrals are evaluated together in isolation from the remaining third. When, however, all three integrals are simultaneously evaluated (taken all together in one numerical bite) the value of acoustic pressure $p(\beta, t)$ on the left side of the equation is finite as the variable T approaches the shock from either side. This finite collective behavior of the three integrals is unexpected and noticed only after the rather tedious derivation of the complete formula [12].

The explanation is simple. When the phase variable T is very close to either side of the shock, all three integrands can be taken together under one double integral, and it can be shown that the combined integrands, added together, are continuous across the shock (whereas each integrand apart from the other two is discontinuous). This continuity follows from the small disturbance shock relations (the demonstration of continuity is itself a tedious algebraic affair). The physical significance of this collectively continuous behavior is that the points on the shock surface are not sources of sound [7]. On the other hand, if the formula were to be further simplified by dropping, for example the quadrupole term, then the points on the shock surface would become acoustic sources—the shock would radiate, but only because the simplification has violated a shock conservation law. It follows that even though equation (5) is in several respects an approximation, any further simplification would result in a loss of essential physics.

There is clearly a computational advantage in the elimination of a volume quadrupole integral in favor of a surface integral. There is, however, a price to pay for this

simplification. The factors $|T-\lambda|^{-1/3}$ and $|T-\lambda|^{-2/3}$ in the two surface integrals will amplify any numerical inaccuracies when both T and λ are near a shock. Also, it is important that the continuity of the summed integrands across a shock is used when T is near the shock and the integration variable λ traverses the shock. But these problems are far easier to handle than the problem of carrying out a full volume integration, especially if the volume includes points off the blade tip. Indeed, if the volume includes a shock, then the same kinds of numerical integration problems must occur when observer and integration variables are near the shock and when they traverse it.

5. COMPARISON WITH THE EXPERIMENTAL DATA

An Euler finite difference solver is used to obtain the flow around a hovering rotor blade [9], assuming that viscous effects are negligible for the high speed rotor impulsive noise. The details of this code which include numerical algorithms and computational grid system are given in the references [9] and [11]. The experimental data were taken with a UH1H rotor blade which has a rectangular planform with the NACA0012 airfoil section [18, 19]. Figure 3 shows the pressure distributions at several positions for the blade tip Mach number of 0·9. Since the blade rotates counterclockwise, the shock appears in the left side of the waveform and bends over to the direction of the freestream with respect to a blade-fixed co-ordinate system. Using this flow field information as an input, the linear Kirchhoff formulation is used to predict the acoustic far-field using several control surface locations. Figure 4 represents the variation of an acoustic planform for different control surface locations. On the control surface located inside the sonic cylinder ($R_{CS}/R = 1{\cdot}05$)

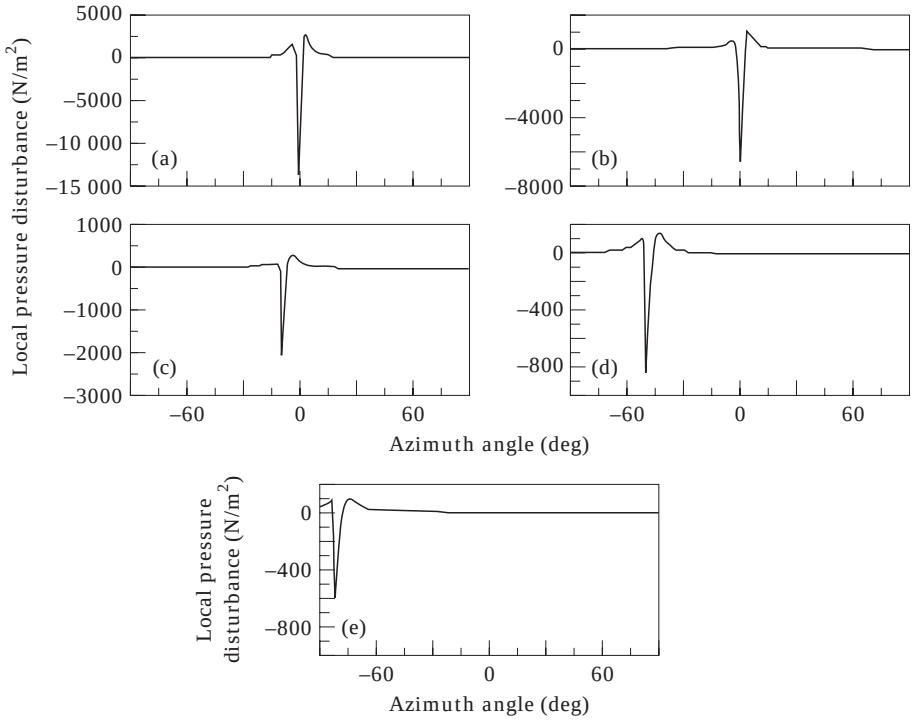

Figure 3. Pressure distributions at several radial positions on the rotor plane at $M_{tip} = 0{\cdot}90$ for R_{cs}/R ratios: (a) 1·05; (b) 1·11; (c) 1·46; (d) 2·41; (e) 3·09.

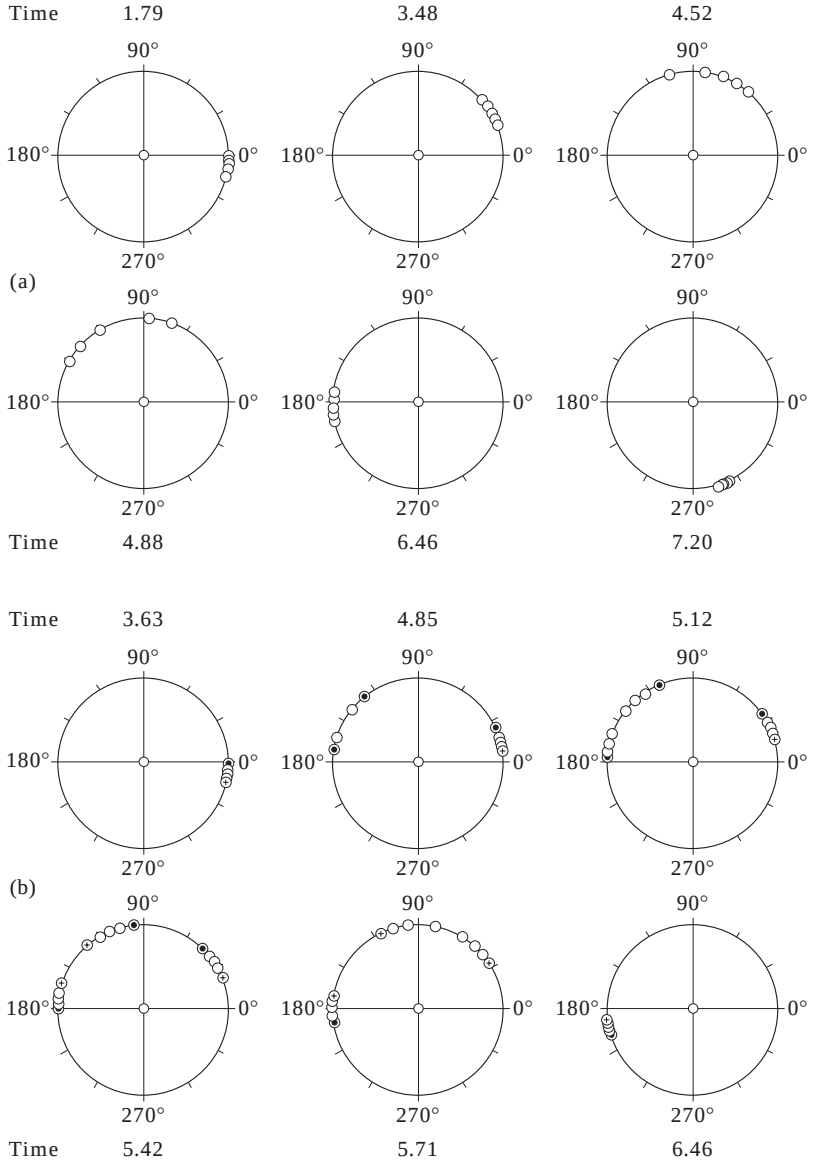

Figure 4. Acoustic planform variation on the control surface for R_{cs}/R ratios of (a) 1·05, inside the sonic cylinder and (b) 1·46, outside the sonic cylinder in case of $M_{tip} = 0{\cdot}90$.

as shown in Figure 4(a), the retarded acoustic planform is enlarged or shrunk as the subsonic radiation Mach number increases (azimuth angles from 0–180°) or decreases (azimuth angles from 180–360°). On the other hand, for a control surface outside the sonic cylinder ($R_{CS}/R = 1{\cdot}46$) as shown in Figure 4(b), the acoustic planform is enlarged and breaks into multiple regions as the Mach number increases and goes beyond unity (sonic speed). Depending on the supersonic radiation Mach numbers at a given observer time, there are several variations of the retarded acoustic planform shapes along the control surface located in a supersonic range as shown at the non-dimensional time of 4·85, 5·42, and 5·71 in Figure 4(b).

Figures 5 and 6 display the pressure distribution and the acoustic signal distribution on the retarded acoustic planform in a supersonic range (Figure 4(b)) at several observer's times. At $t = 4{\cdot}85$, Figure 5 shows a single shock wave around 20° and an overlapping of the two pressure waves around 150°, which correspond to the multiple roots of the retarded time as shown in Figure 4(b). At the same time, the large contribution of the acoustic signal is produced around 150° as shown in Figure 6. On the other hand, at $t = 5{\cdot}42$, the pressure distribution in Figure 5 shows three distinctive peaks which correspond to three roots of the retarded time equation as shown in Figure 4(b). However, the resultant acoustic signal distribution is almost negligible as shown in Figure 6 due to the fact that $\mathrm{d}p/\mathrm{d}n$ and $\mathrm{d}p/\mathrm{d}\tau$ terms cancel each other.

Figure 7 shows the acoustic pressure predictions using the linear Kirchhoff formula with the selected control surfaces located inside or outside of the sonic circle for both hover tip Mach numbers of 0·90 and 0·95. In the cases where the control surface is inside the sonic surface ($R_{cs}/R = 1{\cdot}05$ for $M_{tip} = 0{\cdot}90$; $R_{cs}/R = 1{\cdot}03$ for $M_{tip} = 0{\cdot}95$), the predicted results do not match well with the experimental data. Particularly the predicted waveform shapes are quite symmetric and unlike the experimental data. This discrepancy may be attributed to the fact that the flow field beyond the control surface is still very non-linear and the shock is extended far beyond the control surface.

Now the control surface is enlarged beyond the sonic circle into a supersonic region to capture all the non-linear aerodynamic flow field. The expected results are improved substantially in terms of amplitudes and waveform shapes as the control surface is enlarged until a certain location. At $R_{CS}/R = 1{\cdot}46$, the predicted results match very well with the

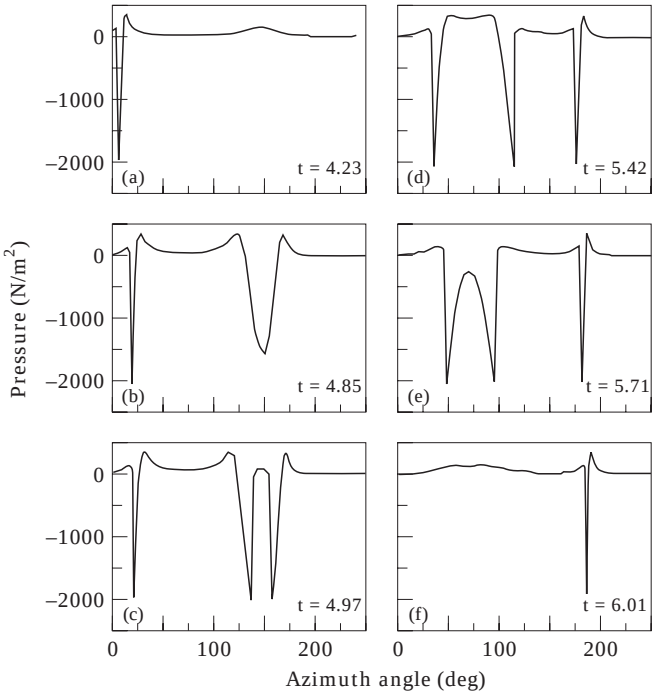

Figure 5. Pressure distributions on the control surface outside the sonic cylinder ($R_{CS}/R = 1{\cdot}46$) at selected observer times (t) in case of $M_{tip} = 0{\cdot}90$: (a) 4·23; (b) 4·85; (c) 4·97; (d) 5·42; (e) 5·71 and (f) 6·01.

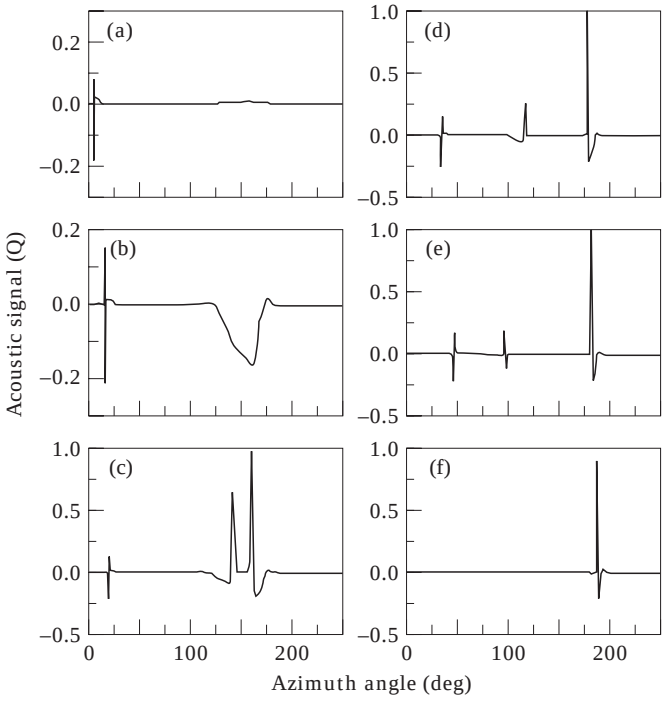

Figure 6. Acoustic signal (Q) distribution on the control circle (at $y = 0$ only) outside the sonic cylinder ($R_{CS}/R = 1{\cdot}46$) at the same observer times as recorded in Figure 5 for $M_{tip} = 0{\cdot}90$. The acoustic signal is calculated from $[Q] = [(\cos\theta/r^2)p - (1/r)\,\partial p/\partial n + (\cos\theta/a_\infty r)\,\partial p/\partial\tau]$.

experimental data in both the amplitude and the waveform as shown in Figure 7. At this particular location, the previous work [10, 11] also showed good correlation with the test data. Further expansion of the control surface beyond this particular location shows the deterioration of the predicted results in waveforms and amplitudes. This may be attributed to the fact that the CFD results may be contaminated by the numerical dissipation.

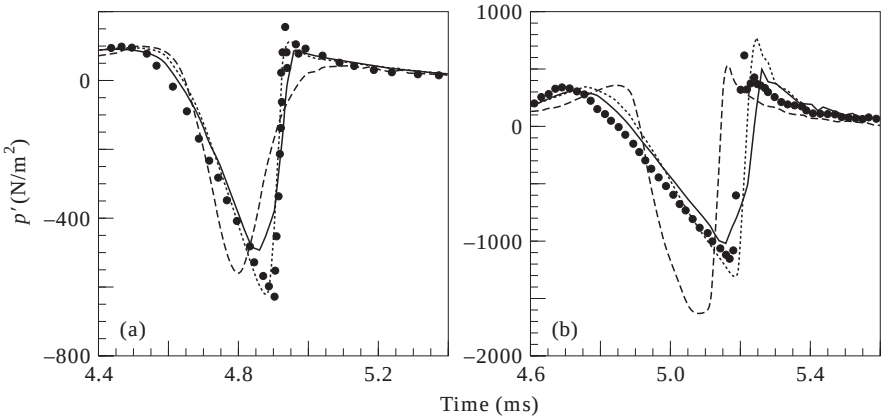

Figure 7. Linear Kirchhoff acoustic pressure prediction at the observer point with respect to the position of the control surface: M_{tip} values; (a) 0·90 and (b) 0·95. Key for R_{cs}/R ratios: ——, 1·03; · · · ·, 1·46; ——, 1·96; ●●●, experimental.

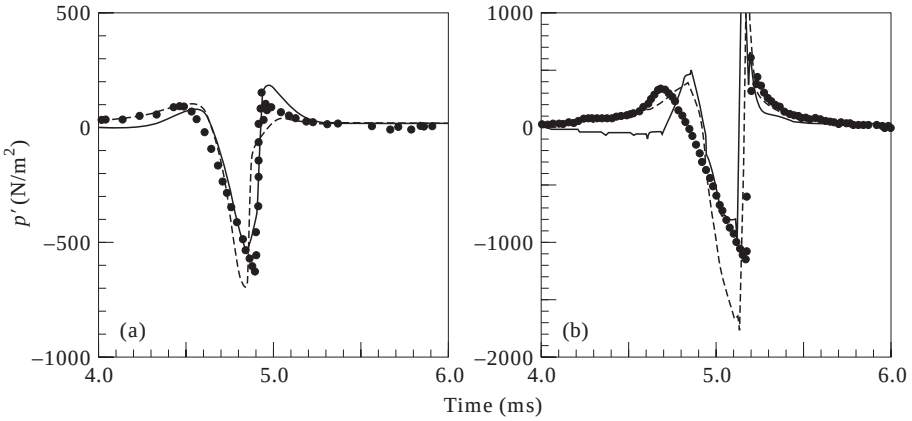

Figure 8. Non-linear Kirchhoff acoustic pressure prediction at the observer point with respect to the position of the control surface for (a) $R_{cs}/R = 1{\cdot}11$, $M_{tip} = 0{\cdot}90$; (b) $R_{cs}/R = 1{\cdot}05$, $M_{tip} = 0{\cdot}95$. Key: ——, Non-linear Kirchhoff; ——, linear Kirchhoff; ●●●, experimental.

In the case of the hover tip Mach number of 0·95 where a strong shock is extended well to the far field, the predicted results show the same trend as of the hover tip Mach number of 0·90. There are still some unanswered questions in this linear Kirchhoff formulation such as the applications of Huygens' principle for supersonic region and the validity of applications of Huygens' principle in the near aerodynamic field.

Calculations based on the non-linear Kirchhoff formula (equation 5) for tip Mach numbers of 0·90 and 0·95 are compared with the experimental data in Figure 8. An extended trapezoidal method is used for the singular integration. Amplitudes and waveforms are in reasonable agreement, even though a numerical singularity problem appears across the shock as previously discussed. This problem can be resolved if a proper analytical expression is used for all three integrands. Also the integration of the non-linear term in equation (5) depends strongly on the shock angle ($\dot{g}$), but there is a difficulty in estimating the shock angle accurately in the numerical solution. The $M_{tip} = 0{\cdot}95$ case is a severe test of the nonlinear formulation because the data surface is only about seven-tenth of a shock from the blade tip. The linear calculation based on the control surface on the sonic cylinder is rather poor. This results support a general conclusion: it is essential to give good account of non-linearity when a Kirchhoff formulation uses a control surface that is close to the blade tip.

6. CONCLUDING REMARKS

Rotor high speed impulsive noise is investigated with a combined CFD–Kirchhoff method and its results are compared with the experimental data for a hovering rotor at high hover Mach numbers. First, the classical linear Kirchhoff formulation is examined in terms of location of control surfaces and the retarded time equation. The results that emerge here are consistent with the basic physics of the flow. When the control surface is well outside of the non-linear aerodynamic flow field, the linear Kirchhoff formulation gives amplitudes and waveforms that agree well with the experimental data. On the other hand, the non-linear Kirchhoff formulation is used for the best advantage when the control surface is very near the blade tip. Then it is the only non-linear formulation that accurately describes the acoustic field.

ACKNOWLEDGMENT

This work has been partially supported by the Agency for Defense Development (TEMD-401-950430) of Korea.

REFERENCES

1. J. E. Ffowcs Williams and D. L. Hawkings 1969 *Philosophical Transactions of the Royal Society* **A264**, 321–342. Sound generated by turbulence and surfaces in arbitrary motion.
2. F. H. Schmitz and Y. H. Yu 1986 *Journal of Sound and Vibration* **109**, 361–422. Helicopter impulsive noise: Theoretical and experimental status.
3. J. Prieur, M. Coster and J. D. Baeder 1991 *International Technical Specialist Meeting on Rotorcraft and Rotor Fluid Dynamics*; *Philadelphia*, *PA*. Aerodynamic and acoustic calculation of transonic nonlifting hovering rotors.
4. F. Farassat and K. Brentner 1988 *Journal of The American Helicopter Society* Jan., 29–36. The use and abuse of the acoustic analogy in helicopter rotor noise prediction.
5. K. J. Schultz and W. R. Splettstoesser 1988 43*rd American Helicopter Society Forum*; *St. Louis*, *MO*. Prediction of helicopter rotor impulsive noise using measured blade pressures.
6. F. Farassat and H. Tadghighi 1990 46*th American Helicopter Society Forum*; *Washington*, *D.C*. Can shock waves on helicopter rotors generate noise?: A study of quadrupole source.
7. M. P. Isom and Y. H. Yu 1991 *International Technical Specialist Meeting on Rotorcraft Acoustics and Rotor Fluid Dynamics*; *Philadelphia*, *PA*. Shock waves and the Ffowcs Williams–Hawkings equation.
8. J. D. Baeder 1989 *Computation and analysis of acoustic waves in transonic airfoil-vortex interactions*. Stanford University. Ph. D. Dissertation.
9. J. D. Baeder 1990 16*th European Rotorcraft Forum Paper No*. II.3.3; *Glasgow*, *Scotland*. Euler solutions to nonlinear acoustics of non-lifting hovering rotor blades.
10. R. Strawn, M. Garceau and R. Biswas 1993 15*th AIAA Aeroacoustics Conference* 93-4359; *Long Beach*, *CA*. Unstructured adaptive mesh computations of rotorcraft high-speed impulsive noise.
11. J. D. Baeder, J. M. Gallman and Y. H. Yu 1993 15*th AIAA Aeroacoustics Conference* 93-4450; *Long Beach*, *CA*. A computational study of the aeroacoustics of rotors in hover.
12. M. Isom, W. Purcell and R. Strawn 1987 11*th AIAA Aeroacoustics Conference* 87-2748; *Sunnyvale*, *CA*. Geometrical acoustics and transonic helicopter sound.
13. B. B. Baker and E. T. Copson 1953 *The Mathematical Theory of Huygens' Principle*. Oxford: Clarendon.
14. F. Farassat and M. K. Myers 1988 *Journal of Sound and Vibration* **123**, 451–460. Extension of Kirchhoff's formula to radiation from moving surfaces.
15. A. S. Lyrintzis and A. R George 1989 *AIAA Journal* **27**, 1451–1453. Use of the Kirchhoff method in acoustics.
16. Y. XUE and A. S. Lyrintzis 1993 49*th Annual Forum of the American Helicopter Society*; *St. Louis*, *MO*. The use of a rotating Kirchhoff formulation for 3-d transonic BVI far-field noise.
17. Y. H. Yu and F. H. Schmitz 1980 6*th AIAA Aeroacoustics Conference* 80-1009; *Hartford*, *Connecticut*. High-speed rotor noise and transonic aerodynamics.
18. T. W. Purcell, R. C. Strawn and Y. H. Yu 1987 *AHS Specialists Meeting on Aerodynamics and Aeroacoustics*; *Arlington*, *Texas*. Prediction of high-speed rotor noise with a Kirchhoff formula.
19. T. W. Purcell 1988 *Fourteenth European Rotorcraft Forum*; *Milano*, *Italy*. CFD and transonic helicopter sound.

APPENDIX: NOMENCLATURE

a_∞	speed of sound in undisturbed air
M_{tip}	blade tip Mach number
$\hat{\mathbf{n}}$	normal vector on the surface
p	perturbed pressure
$\hat{\mathbf{r}}$	radiation vector
R	distance between a source position at the sound generation time and an observer at the sound receiving time *or* length of blade
R_{cs}	radius of control surface
R_{ob}	distance from the hub to the observer
t	observer time
T	phase variable

x blade co-ordinate
$\hat{\mathbf{x}}, \hat{\mathbf{y}}$ location vectors
Z_0 scaled vertical distance
β distance to an observer along a line tangent to the sonic cylinder
ε inverse of the aspect ratio
γ specific heat ratio
Ψ respective azimuth angle of the source positions at sound generation time
ρ_0 density of undisturbed air
λ integration variable
Ω angular speed of the blade
τ retarded time
θ angle between the normal vector on the surface and the radiation vector *or* cylindrical polar angle in a blade-fixed co-ordinate in radians
θ_s angle between the vector normal to the sonic circle and a shock